NIH Public Access
Author Manuscript
J Bioenerg Biomembr. Author manuscript; available in PMC 2013 April 01.

Published in final edited form as:
J Bioenerg Biomembr. 2012 April ; 44(2): 253–263. doi:10.1007/s10863-012-9427-2.

Quantitative Imaging of Mitochondrial and Cytosolic Free Zinc Levels in an *in vitro* Model of Ischemia/Reperfusion

Bryan J. McCranor[1], **Rebecca A. Bozym**[1], **Michele I. Vitolo**[1,2], **Carol A. Fierke**[3], **Linda Bambrick**[4], **Brian M. Polster**[4], **Gary Fiskum**[4], and **Richard B. Thompson**[1,*]

[1]Department of Biochemistry and Molecular Biology, University of Maryland School of Medicine, 108 N. Greene St., Baltimore MD 21201

[2]University of Maryland Marlene and Stewart Greenebaum NIH Cancer Center

[3]Department of Chemistry, University of Michigan, 930 N. University Ave., Ann Arbor MI 48109

[4]Department of Anesthesiology and the Center for Shock, Trauma, and Anesthesiology Research, University of Maryland School of Medicine, 685 W. Baltimore St., Baltimore MD 21201

Abstract

The role of zinc ion in cytotoxicity following ischemic stroke, prolonged status epilepticus, and traumatic brain injury remains controversial, but likely is the result of mitochondrial dysfunction. We describe an excitation ratiometric fluorescence biosensor based on human carbonic anhydrase II variants expressed in the mitochondrial matrix, permitting free zinc levels to be quantitatively imaged therein. We observed an average mitochondrial matrix free zinc concentration of 0.2 *pM* in the PC12 rat pheochromacytoma cell culture line. Cytoplasmic and mitochondrial free zinc levels were imaged in a cellular oxygen glucose deprivation (OGD) model of ischemia/reperfusion. We observed a significant increase in mitochondrial zinc 1 hr following 3 hr OGD, at a time point when cytosolic zinc levels were depressed. Following the increase, mitochondrial zinc levels returned to physiological levels, while cytosolic zinc increased gradually over a 24 hr time period in viable cells. The increase in intramitochondrial zinc observed during reoxygenation after OGD may contribute to bioenergetic dysfunction and cell death that occurs with both *in vitro* and *in vivo* models of reperfusion.

Keywords

zinc; oxidative stress; mitochondria; ischemia; stroke; fluorescence biosensor; ratiometric; carbonic anhydrase II

INTRODUCTION

Ischemia is the result of cessation of perfusion and the root cause of all stroke cases, mostly originating from blockage of an intra-cranial artery by a blood clot [1]. While a significant cause of death, stroke causes disability more often than morbidity: a third of all stroke survivors are functionally dependent a year afterwards and stroke ranks as the second most frequent cause of dementia, a prominent cause of depression, and the number one cause of epilepsy in the elderly. Despite the introduction of tissue plasminogen activator and other therapies and interventions which have reduced stroke incidence in some areas [2], effective treatment for many strokes (or even rapid diagnosis and localization of the insult) still remains to be developed.

*to whom correspondence should be addressed: rthompso@umaryland.edu; Phone (410) 706-7142, fax (410) 706-7122.

$watermark-text

$watermark-text

$watermark-text

Several studies of ischemia have indicated that zinc ion plays a role in subsequent neuronal death [3,4] (reviewed in [1,5], Thompson (in the press)). Even nanomolar zinc levels were observed early on to be toxic to neurons in culture [6], and in some systems elevated zinc induces apoptosis[7,8] [9], whereas other investigators have found that apoptosis induced by addition of zinc chelators can sometimes be rescued by zinc addition [10] [11,12]. Furthermore, several investigators have observed substantial increases in extracellular and intracellular free zinc concentrations following ischemia and ischemic-like events [13–17] and degenerating neurons have been reported to exhibit an increase in intracellular zinc [18,19,8,20]. Some have proposed that this increase is due to uptake from extracellular sources (notably presynaptic vesicles of a subset of glutamatergic neurons) whereas others believe that the zinc is released from intracellular sources. Another widely observed consequence of ischemia/reperfusion injury is an increase in mitochondrial dysfunction. Ischemic insults result in increased reactive oxygen species (ROS) production, decreased ATP production, activation of mitochondrial permeability transition (MPT), and activation of pro-apoptotic signals [21]; [22,23] [24] [25]. These severe consequences suggest that the integrity of mitochondrial function may well determine overall cellular viability following ischemia/reperfusion. Zinc ions in the sub-micromolar range can directly inhibit key mitochondrial enzymes necessary for energy production such as lipoate-linked dehydrogenases, leading to an increase of ROS production and mitochondrial dysfunction; in addition, zinc ion is a potent inhibitor ($K_i \approx$ nanomolar) of enzymes such as glutathione reductase and thioredoxin reductase, which are key to detoxification of reactive oxygen species [26] [27,28]. Therefore, it would not be surprising if mitochondrial free zinc is under tight control and kept at low concentrations. Consequently, any increase in mitochondrial free zinc, following ischemia/reperfusion, could play a substantial role in the increase in ROS production, decrease in ATP production, and overall mitochondrial dysfunction associated with ischemia/reperfusion injury.

Previously, we described an excitation ratiometric fluorescence biosensor for zinc ion based on human carbonic anhdrase II that exhibits very high affinity and selectivity, and may be inserted into or expressed in cells [29–32] [33]. The excitation ratiometric feature avoids common artifacts which compromise accuracy when using simple intensity-based fluorescent indicators in cells, due to variations in cell thickness or loading, washout, or photobleaching, while being usable in ordinary fluorescence microscopes. Moreover, the long emission wavelength of the biosensor (~ 617 nm in this example) avoids the need to correct for autofluorescence of the cells or media. We have demonstrated that the selectivity, sensitivity, and response speed of the biosensor can all be improved by subtle mutagenesis of the protein [34–36]. Our Förster resonance energy transfer (FRET) based system thus allows for free zinc measurements at picomolar levels [30] in live resting cells at physiological levels [37]. “Free zinc” (or labile zinc) in the cell includes dissolved zinc ion species bound with weak, rapidly exchangeable ligands such as water or chloride ion [38]; in cells, most zinc ion is tightly bound by proteins, peptides and amino acids [39] [40,41], and is essentially undetected by most indicators, including our biosensor.

The zinc biosensor can be readily inserted into cells via a TAT protein transduction domain [37], but to study mitochondrial zinc we devised an expressible CA II-fluorescent protein fusion which may be targeted to the organelle using the mitochondrial localization sequence of subunit 8 of cytochrome oxidase (Complex IV) in the electron transport chain. We demonstrate that the probe localizes in the mitochondrial matrix, where we can image the free zinc concentration with picomolar affinity. While others have described fluorescent indicators that respond to zinc and localize in the mitochondrion [42] [43], as well as expressible [44] and ratiometric indicators [45], our biosensor has sufficient sensitivity and selectivity to measure mitochondrial matrix zinc at resting levels. The biosensor was calibrated *in situ* in isolated mitochondria and its matrix location confirmed. Several lines of

$watermark-text

$watermark-text

$watermark-text

evidence described above suggest that under ischemic conditions free zinc levels are elevated and contribute to cellular damage; we have now quantitatively imaged free zinc levels in an *in vitro* ischemia/reperfusion model following the insult. PC-12 cells were subjected to an oxygen glucose deprivation (OGD) model of ischemia [46] which resulted in approximately 50% cell death 24 hr after the end of OGD and their cytoplasmic and mitochondrial free zinc levels were imaged as a function of time following the insult.

METHODS

Reagents and Materials

The pDsRed2-Mito vector was obtained from Clontech (Mountain View, CA). Lipofectamine 2000, OPTI-MEM media, Neurobasal-A media, B-27 supplement and MitoTracker Green FM were purchased from Invitrogen (Carlsbad, CA). Digitonin was from Sigma-Aldrich (St. Louis, MO). Goat *anti*-Mouse IgG Dylight$_{TM}$ 405 Conjugated was from Pierce Biotechnology (Rockford, IL). Mouse *anti*-TOM20 antibody was from BD Bioscience (San Jose, CA). Rabbit *anti*-COX IV monoclonal antibody (Alexa Fluor 488 Conjugated) was from Cell Signaling Technology (Danvers, MA). FCCP (carbonyl cyanide 4-(trifluoromethoxy)phenylhydrazone) was from Enzo Life Sciences (Plymouth Meeting, PA). PC12 cells were obtained from ATCC (Manassas, VA). FluoroDish 35 *mm* glass bottomed tissue culture dishes were from WPI Inc. (Sarasota, FL). All other chemicals and reagents were obtained from common commercial sources.

Construction, Expression, and Labeling of TAT-H36C-CA Cytoplasmic Sensor

This sensor was chosen to measure cytoplasmic zinc concentrations because it exhibits almost 20-fold weaker zinc affinity (K_D =70 pM) than the wild type [37], extending upward the dynamic range of zinc concentration which it can measure accurately. The construction and fluorescent labeling of the TAT conjugated H36C variant of carbonic anhydrase were as previously described [37]. There was no further modification of the probe in this study.

Construction of the CA-DsRed Mitochondrial Sensor

The gene for human carbonic anhydrase II (CA) was amplified using PCR with the following primers: sense primer, 5′-CCGCGCGCCAAAGATCCATTCGTTGATGGCCCATCACTGGGGGTACGGC-3′, containing a BssHII site, and antisense primer, 5′-CATCGGAATCCCCACCTTTGAAGGAAGCTTTG-3′. This CA gene was cloned into the BssHII and blunted BamHI sites of the pDsRed2-Mito vector. The pDsRed2-Mito/CA vector contains the CA gene in frame with an upstream mitochondrial localization signal sequence (from subunit VIII of human cytochrome c oxidase) and a downstream DsRed2 gene. The insert and the expression vector were sequenced to ensure no deleterious mutations had occurred.

Cell Culture

PC12 cells were cultured in Neurobasal-A media minus Phenol Red, supplemented with 2% B-27 supplement, 0.5 *mM* L-Glutamine, and 1% Penicillin-Streptomycin. Prior to experiments PC12 cells were re-plated on 35 *mm* glass bottomed culture dishes (World Precision) to allow for better imaging.

Cellular Transfection

PC12 cells were transfected according to the Lipofectamine 2000 manufacturer's protocol (Invitrogen), using 10 μg of DNA per 35 *mm* culture dish. Cells were transfected for 24 hrs and were used for imaging following another 24 hr period.

$watermark-text

$watermark-text

$watermark-text

Mitochondria Isolation

Approximately 7.2×10^8 transfected cells were removed from T-75 flasks by trypsinization and quickly resuspended in 10 ml of Dulbecco's phosphate buffered saline (DPBS) containing 5 mg of trypsin inhibitor (0.5 mg/ml). The cells were further diluted by again adding 10 ml of DPBS and centrifuged at 800*g* for 5 minutes. The supernatant was removed and cells were resuspended in ice-cold MS buffer (225 mM mannitol, 75 mM sucrose, 5 mM HEPES, 1 mg/ml fatty acid free BSA, pH 7.4) containing 1 mM EGTA and centrifuged at 1,000*g* for 5 minutes. The supernatant was again aspirated and cells were resuspended in ice-cold MS buffer + EGTA. The cellular membrane was then disrupted by the addition of 14.4 μl digitonin from a 10% stock solution to the cells, while stirring for 30 seconds. Additional MS buffer and EGTA were then added to the cells to dilute out the digitonin and the cells were centrifuged at 4,000*g* for 3 minutes at 4°C. The supernatant was aspirated and the loose pellet was poured into a Dounce homogenizer. The pellet was homogenized in MS buffer + EGTA, then centrifuged at 2000*g* for 5 minutes at 4°C. After centrifugation the top layer of the supernatant was collected and centrifuged at 14,000*g* for 10 minutes at 4°C. The resulting brown mitochondrial pellet was collected and resuspended in MS buffer +EGTA and centrifuged again at 14,000*g* for 10 minutes at 4°C. The supernatant was then aspirated and the mitochondrial pellet was resuspended in a single drop of MS buffer without EGTA.

Sensor Calibration in Isolated Mitochondria

Approximately 0.45 *ng* of isolated mitochondria were plated in a 35 *mm* glass bottomed dish and incubated at 37°C, 5% CO_2 for 20 minutes. The mitochondria were then incubated with 250 μl each of a series of artificial cerebrospinal fluid (ACSF) zinc buffers pH 7.4, having concentrations of free zinc calculated by MINEQL (Environmental Research Software, Hallowell, ME), for 40 min at 37°C, 5% CO_2. After 40 minutes of incubation 1 μM of dapoxyl sulfonamide was added to the mitochondria, which were then allowed to incubate for an additional 20 minutes at 37°C, 5% CO_2, prior to imaging.

Sensor Co-localization with Mitochondria

To establish co-location of the sensor with the mitochondrion, cells expressing the sensor were also stained with a mitochondrion-specific fluorophore, Mitotracker Green. PC12 cells were transfected as described above, and a fraction was plated on 35 mm glass bottomed dishes while the other fraction underwent mitochondrial isolation also as described above. Transfected PC12 cells were incubated with 0.02 μM Mitotracker® Green FM (Invitrogen) for 30 min at 37°C, 5% CO_2, and then washed and imaged using a Nikon Eclipse TE-300 epifluorescence microscope (see below) at excitation and emission wavelengths of 540 *nm* and 617 *nm*, respectively (DsRed2 fluorescence), and also with 490 *nm* excitation and 516 *nm* emission (Mitotracker® fluorescence). Images were then merged in IPLab software (Scanalytics, Inc.) to determine co-localization.

Sensor Localization Within Mitochondria

The sensor position with respect to the mitochondrial outer membrane and inner membrane was established by fluorescence colocalization using fluorescent antibodies that recognize proteins specific to the compartments. Isolated mitochondria were split into two groups: one group underwent inner mitochondrial membrane isolation while the other was left untreated. The inner mitochondrial membrane was isolated by dilution with equal parts of a 2% digitonin stock in 0.25 *M* sucrose solution, which effectively solubilizes the cholesterol-containing outer membrane without solubilizing the cholesterol-poor inner membrane. The resulting inner membrane vesicles (mitoplasts) were stirred gently on ice for 15 min, and then further diluted with 3 volumes of 0.25 *M* sucrose. The mitochondria were then centrifuged for 10 min at 9500*g.* The supernatant was removed and saved, and the pellet

$watermark-text

$watermark-text

$watermark-text

containing the matrix confined by the inner membrane was resuspended in the sucrose solution and centrifuged for 10 min at 9500*g*. Again, the supernatant was removed and combined with the prior fraction, and the pellet was resuspended in a small amount of sucrose solution. Intact mitochondria and inner membrane fractions were each plated on a 35 *mm* glass bottomed dish, and then incubated at 37°C, 5% CO_2 for 30 min. 2 μl of Goat Anti Mouse IgG conjugated with Dylight$_{TM}$ 405 and 2 *ul* of Mouse Anti-TOM20 antibody specific for the outer membrane protein TOM20 were diluted in 1 *ml* of MS Buffer and 1 *ml* of 0.25 *M* sucrose. 10 μl of Alexa Fluor 488-conjugated rabbit mAb specific for the COX IV protein of the mitochondrial inner membrane was diluted in 1 *ml* of MS Buffer and 1 *ml* of 0.25 *M* sucrose. An aliquot of 200 *ul* of each antibody solution was added to both the isolated mitochondria and inner mitochondrial membrane fractions, which were then incubated for 30 min at 37°C, 5% CO_2. Images were taken at corresponding wavelengths for DsRed2, Dylight 405, and Alexa Fluor 488 and merged as above to determine co-localization.

To determine if the sensor was localized within the mitochondrial matrix, the pH sensitivity of the sensor was utilized: addition of the proton ionophore/uncoupler carbonylcyanide-*p*-trifluoromethoxyphenylhydrazone (FCCP) to respiring mitochondria results in a rapid decline in mitochondrial matrix pH which correspondingly reduces the zinc-binding affinity of the sensor [47]. Thus, if the sensor exhibits an abrupt drop in ratio following FCCP treatment, it most likely resides in the matrix since the pH of the intermembrane space or the extramitochondrial milieu is unaffected by respiratory uncoupling. Transfected PC12 cells were also incubated for 5 min with 1 μM Dapoxyl sulfonamide at 37°C, 5% CO_2 before 0.5 μM FCCP dissolved in DMSO was added. Cells were incubated for an additional 15 min and then imaged at Excitation 365 *nm*/Emission 617 *nm* and Excitation 540 *nm*/Emission 617 *nm*. A ratio of Ex365*nm*/Ex540*nm* was calculated using IPlab software (Scanalytics Inc.) to determine the effect of FCCP on zinc binding.

Hypoxia and hypoglycemia study

As a model of ischemia and reperfusion, cultured PC-12 cells were subjected to oxygen and glucose deprivation, followed by incubation in 95%/5% air/CO_2 [46]. For mitochondrial OGD imaging, PC12 cells were transfected as described above. Two days prior to the experiments a zinc- and glucose-free artificial cerebrospinal fluid (ACSF), pH 7.4 (0.142 *M* NaCl, 0.005 *M* KCl, 0.001 *M* $MgCl_2$•$6H_2O$, 0.002 *M* $CaCl_2$•$4H_2O$, 0.01 *M* HEPES, and 50 μM Bicine) was deoxygenated in an Anaerobic System (Forma Scientific, Model #1025) in 85% N_2, 10% H_2, 5% CO_2 with approximately one ppb oxygen. On the day of the experiment PC-12 cells plated on 35 *mm* glass bottomed culture dishes were placed in the anaerobic chamber and Neurobasal-A medium was replaced with the deoxygenated zinc- and glucose-free ACSF [48]. The cells were then incubated in the chamber for 3 hours. Following the incubation, the cells were washed three times, supplemented Neurobasal-A media (containing glucose) was added back to the cells, and they were then incubated for 24 hours at 37°C, 95% air, 5% CO_2.

Cell staining

For intracellular imaging, cells were stained by immersion in a zinc-free isotonic medium [49] containing 1 μM Alexa Fluor 594-labeled apo-TAT-H36C-CA and 1 μM Dapoxyl sulfonamide (dissolved in DMSO) and imaged as described previously by Bozym, et al,. [37]. For mitochondrial imaging of transfected cells only 1 μM dapoxyl sulfonamide was added to the cells, which were then incubated for 25 min at 37°C in 5% CO_2. Cells were imaged without washing, in the presence of 1 μM Dapoxyl sulfonamide. Cytosolic zinc images were performed in the presence of Trypan blue staining to ensure that only viable cells were imaged.

$watermark-text

$watermark-text

$watermark-text

Cell imaging

Cells were photographed using a Nikon Eclipse TE300 epifluorescence microscope with a D540/25X or a D360/40X excitation filter, 570DCXRU dichroic and D630-30M barrier filter (all Omega), through a Nikon Plan Fluor 100x oil/1.3 NA objective with a Cooke Sensicam QE cooled CCD camera. Images were captured using IPLab software (Scanalytics, Inc.). To determine the fluorescence ratio for cells, the images for each excitation ratio were divided and a ratio image was created. Pixels corresponding to the sensor emission (with green excitation) were selected by IPLab software based on relative intensity. The same pixels were then selected in the ratio image to calculate the mean ratio for each image.

RESULTS AND DISCUSSION

Mitochondria Probe Calibration and Localization

Calibration of the sensor under conditions as similar to the living cell as possible is important to obtain accurate results. While *in situ* calibration is frequently done in cells for calcium indicators, it has been demonstrated in several cell lines that free zinc ion concentrations above or below a narrow concentration band are toxic [9], and thus such a calibration would be difficult. In view of the widespread use of isolated mitochondria for studying their function, calibrating the sensors in isolated mitochondria was thus most appropriate for this purpose. A plot of the calibration curve of the sensor in unenergized isolated mitochondria in zinc-buffered saline reveals an apparent K_d of 0.15 ± 0.05 *pM* (Figure 1). This is lower than the K_d of wtCA-DsRed2 in pH 7.4 zinc-saline buffers (17 pM) and substantially lower than the K_d reported previously [37] for the TAT tagged H36C-AF594-CA probe used for imaging intracellular zinc. The lower K_d is attributable to the high solute levels in the mitochondrion and correspondingly low water activity, which would shift the zinc ion dissociation equilibrium towards the bound rather than the (hydrated) free ion. The exact values of the ratios can vary with the quantum yield of the bound Dapoxyl sulfonamide, which in turn may vary with the altered conditions inside the mitochondrion. The dynamic range of the mitochondrial sensor, wherein the zinc level can be measured with reasonable accuracy, extends roughly from 0.02 *pM* to 2 *pM*.

We also confirmed that the expressible mitochondria sensor was correctly targeted, by incubating transfected PC12 cells with Mitotracker Green FM, a dye that selectively localizes to the mitochondria. Merged images of both DsRed2 (red fluorescence) and Mitotracker emission (green fluorescence) reveal their co-localization in the mitochondria by yellow color (Figure 2A). While the co-localization with Mitotracker indicates that the CA-DsRed2 sensor is expressed on or in the mitochondria of transfected cells, standard fluorescence microscopy has insufficient resolution to determine whether the sensor is located within the matrix, the intermembrane space, or bound to the inner or outer membranes To determine where it is expressed, isolated intact mitochondria and isolated mitochondria with the outer membrane removed by digitonin treatment were probed with fluorescent-labeled antibodies specific for proteins present on the inner (COX IV, a cytochrome oxidase subunit) and outer (Tom20, translocase of outer mitochondrial membrane 20) mitochondrial membranes. Incubations with the TOM20 and COX IV antibodies reveal that the CA-DsRed2 probe is being expressed in the inner membrane or matrix of the mitochondria in transfected cells (Figure 2B), since the DsRed2 fluorescence of the sensor colocalized with the fluorescence of the anti-TOM20 antibody in the absence (but not the presence) of digitonin treatment, and with the fluorescence of the anti-COX IV antibody following digitonin treatment and centrifugation. To test if the sensor is expressed on the matrix side of the inner mitochondrial membrane as expected, rather than the outer surface of the inner membrane, we observed the effect of FCCP on the reported ratio. By

$watermark-text

$watermark-text

$watermark-text

acting as a proton ionophore which uncouples oxidative phosphorylation from ATP synthesis by creating a "proton leak" back into the matrix, FCCP causes a rapid drop in intra-mitochondrial pH shortly after administration. The drop in pH will cause a decrease in the sensor zinc affinity [47], which will be observed as a decrease in the fluorescence ratio. The observed significant ($p \leq 0.05$) decrease in ratio of excitation 365 *nm*/excitation 540 *nm* in cells incubated with 0.5 μM FCCP for 15 min (0.48 ± 0.22), as compared with control cells (0.63 ± 0.11) indicates the sensor is imaging mitochondrial matrix zinc. This is unsurprising since the targeting sequence used comes from subunit VIII of cytochrome c oxidase, a matrix protein.

Intracellular and Intra-mitochondrial Zinc Imaging

Previously we had reported imaging intracellular zinc in PC12 cells under physiological conditions using a ratiometric indicator. From the images it was determined that the average intracellular concentration of labile zinc was around 10 *pM,* which is somewhat less than reported by other laboratories [41] [50–52] (summarized in Haase and Rink's excellent review [53]) Specifically, these investigators measured levels between 0.17 and 1 nanomolar free zinc in various cell types (including PC-12 cells) using the fluorescent indicator FluoZin-3. We note that FluoZin-3 is not ratiometric and exhibits a K_D of 15 nM [42], which makes accurate determination of subnanomolar levels in cells by microscopy challenging. Other workers obtained results in the subnanomolar range with Fura-2 [54,55] and nanomolar range with Mag-Fura-5 [56], but potential competition from endogenous Ca and Mg, respectively, complicates interpretation when using these indicators [57]. Merkx's group points out [58] that 10 pM is near the bottom of the dynamic range with that CA-based sensor and thus the measurement cannot be very precise; while this critique is correct, it is equally clear from this earlier measurement that the free zinc concentration in the cytoplasm of these cells is not 170 pM since this concentration should nearly saturate the wild-type CA-based cytoplasmic sensor and this is not observed using either the TAT-tagged Alexa Fluor 594-labeled wild type apo CA or E117A CA in eukaryotic PC-12 cells, Chinese hamster ovary cells [37], nor retinal pigmented epithelial ARPE-19 cells (McCranor and Thompson, in preparation), nor the expressible DsRed2-apoCA (wild type) (Bozym and Thompson, unpublished results). Most recently, Qin, et al., [59] measured free zinc concentrations in the Golgi and endoplasmic reticulum compartments of HeLa cells using a targeted expressible sensor and found significantly lower levels (0.6 and 0.9 pM, respectively) in these organelles. Wang, et al., [33] find somewhat higher (20–30 pM) resting levels in *E. coli* using a similar CA-based sensor, and the level varies with extracellular zinc concentration. It does not seem unreasonable that different cell types under varying conditions may in fact have different free zinc concentrations. In this study we imaged intra-mitochondrial zinc using our expressible Mito-CA-DsRed2 sensor to determine the concentration of mitochondrial labile zinc. The sensor reports that, in the mitochondria of PC12 cells under physiological conditions, the average concentration of labile zinc is around 0.15 *pM* (Figure 3 upper left).

This number does not necessarily indicate that there is less total zinc in the mitochondrion, rather, it more likely indicates that the matrix contains substantial concentrations of zinc ligands which strongly buffer the free zinc. Note that there is quite substantial variability apparent within even individual cells; it is unclear whether this represents variability in the free zinc concentration, the population of zinc ligands, or both.

Zinc Imaging following OGD

In order to mimic the effects of ischemia/reperfusion injury *in vitro,* an OGD model was employed. PC12 cells were subjected to 3 hours of OGD to model ischemia, followed by an additional incubation period (1 hr, 2 hr, 14 hr, or 24 hr) under normal conditions (37°C, 95%

$watermark-text

$watermark-text

$watermark-text

air, 5% CO_2) to model reperfusion. An incubation of 24 hr after 3 hr OGD resulted in approximately 50% dead cells as judged by Live/Dead cell staining [46] (data not shown). Zinc images with the TAT-H36C-CA probe reveal a significant increase in cytoplasmic free zinc 24 hrs after OGD (>100 *pM*) as compared to control cells (10 *pM*) (Figure 4, 5). Interestingly, this increase is gradual and follows a period of significantly decreased cytosolic zinc at 1 hr after OGD (0.9 *pM*) (Figure 4). Again, the cells show increased variability in cytoplasmic zinc levels following OGD as well as (in some cases) reduced nuclear free zinc (Figure 4, bottom right). At the same time cytosolic zinc is depressed, mitochondrial matrix zinc levels show a substantial increase (to >10 *pM*) over control levels (0.2 *pM*) in the first hour after OGD cessation (Figure 3, 5); the actual level is not measured very precisely since it is near the top of the sensor dynamic range. However, the surge in mitochondrial free zinc is short lived and by 2 hrs after OGD it was back down around physiological levels. At later time points, 14 hr and 24 hrs after OGD, there a slight increase in mitochondrial zinc is observed, but these increases are not significant and may be due to increased prevalence of non-viable cells.

Discussion

We have developed an expressible ratiometric carbonic anhydrase-based fluorescent indicator system that allows us to quantitatively image free zinc ion in the cytoplasm and specifically in the mitochondrion. We found that the cytoplasmic biosensor gave similar results to those we had previously obtained in other cell types [37]. Using this approach we found that the average mitochondrial labile zinc in PC12 cells is in the range of 0.15 *pM*. This is less than the levels observed in the cytosol, but perhaps unsurprising considering the deleterious effects free zinc can have on mitochondrial function [4] [27,28]. We used the biosensors to quantitatively image the changes in intracellular and intra-mitochondrial zinc concentrations in undifferentiated PC12 cells subjected to oxygen + glucose deprivation as a model of ischemia/reperfusion. In both cases the increase in labile zinc was substantial, although at different time points in the study. Over the long term cytosolic zinc is increased in viable cells following OGD, but during the short term (1 hr after OGD) cytosolic zinc levels are depressed. At one hour mitochondrial matrix zinc levels are increased substantially (>10 *pM*), although this measurement is near the top of our dynamic range. The increase is brief, however, and matrix zinc levels are back nearly at physiological levels by 2 hrs after OGD.

What is the origin of the zinc changes observed in the cytoplasm and mitochondria? In neuronal models of excitotoxicity, zinc ion can enter cells from the extracellular space through NMDA receptors or AMPA/kainite channels [60,61]; in this case, while there is higher external free zinc in the medium (≈ 5 nanomolar), there is no glutamate or glutamate analog agonist present to open such channels, so it seems unlikely the cytoplasmic changes occur as a result of zinc movement across the plasma membrane. Zinc can be released from intracellular ligands by at least two mechanisms which are likely to occur during ischemia and reperfusion. The first is oxidation of sulfur ligands on molecules like glutathione, cysteine, and proteins like metallothionein and zinc fingers that bind zinc using cysteine side chains, particularly oxidation of thiols to form disulfides. Oxidation of glutathione during ischemia has been observed (reviewed in [62]) and helps quench reactive oxygen species that are present. The second is release of zinc from histidinyl imidazole ligands by protonation due to acidosis of the tissue. The acidosis arises from lactate production from pyruvate under anaerobic conditions; the brain pH declines as low as 6.0 in models of global ischemia [63], which protonates histidine residues, reducing their affinity for zinc ions. However, in our model of adherent PC-12 cells (essentially a monolayer) in excess buffered medium, there is likely little change in the pH, so we do not believe this mechanism is important in this case. Finally, we note that several groups have observed release of granular

$watermark-text

$watermark-text

$watermark-text

zinc in hippocampal slice preparations following ischemia; since the chemical makeup of the granules remains to be elucidated, the mechanism for the release is unclear. Although the PC-12 cell line is widely used to model neurons (and was chosen in part for this reason), they contain no granular zinc. Thus we conclude that the changes in free zinc ion in our system are largely due to oxidation/reduction of thiol zinc ligands. While we would propose that the elevated levels of zinc in the mitochondrion immediately after OGD cessation are due to release from GSH converted to GSSG and the subsequent decline due to re-reduction of the glutathione, the reasons for the subsequent (modest) increase above normal are unclear. By comparison, there is no ready explanation for the drop in cytoplasmic free zinc following cessation of the insult, nor the steady, significant increase thereafter. It may be that slower process(es) initiated during OGD are operating and result in a release of zinc from intracellular sites. One possibility is that apoptosis (a process that takes hours) initiated during ischemia has resulted in proteolysis of intracellular zinc-binding proteins, releasing bound zinc; we and others have found apoptosis initiated by agents such as staurosporine results in elevated free zinc in cells prior to their death (results not shown).

These data support other studies referred to above which have observed increases in zinc following ischemia reperfusion injury. Whether the observed increase in mitochondrial matrix zinc is due to an uptake of zinc from the cytosol or a release of zinc from mitochondrial ligands is not known at this time. The results indicate that dramatic changes in zinc homeostasis occur as soon as 1 hr after oxygen/glucose deprivation, with differing effects in the cytosol and mitochondria. These changes in zinc concentrations can have a serious effect on overall cell viability, as others have observed, and further implicate zinc as potential cause of cell death following ischemia/reperfusion injury.

Acknowledgments

The authors gratefully acknowledge the National Institutes of Health (NIBIB RO1 EB03924 (R.B.T., B.J.M., R.A.B., C.A.F.); PO1 HD16596-25 (G.F., L.H.); NINDS RO1 NS064978 (B.M.P.) and the Susan G. Komen Breast Cancer Foundation (PDF 0601045 (M.I.V.) for their support. The fluorescence sensing technology was originally developed with support from the Office of Naval Research.

References

1. Galasso SL, Dyck RH. The role of zinc in cerebral ischemia. Molecular Medicine. 2007; 13(7–8): 380–387.10.2119/2007-00044.Galasso [PubMed: 17622314]
2. Rothwell PM, Coull AJ, Giles MF, Howard SC, Silver LE, Bull LM, et al. Change in stroke incidence, mortality, case-fatality, severity, and risk factors in Oxfordshire, UK from 1981 to 2004 (Oxford Vascular Study). The Lancet. 2004; 363(9425):1925.
3. Bossy-Wetzel E, Talantova MV, Lee WD, Scholzke mN, Harrop A, Mathews E, et al. Crosstalk between nitric oxide and zinc pathways to neuronal cell death involving mitochondrial dysfunction and p38-activated K+ channels. Neuron. 2004; 41:351–365. [PubMed: 14766175]
4. Jiang D, Sullivan PG, Sensi SL, Steward O, Weiss JH. Zn2+ induces permeability transition pore opening and release of pro-apoptotic peptides from neuronal mitochondria. Journal of Biological Chemistry. 2001; 276:47524–47529. [PubMed: 11595748]
5. Shuttleworth CW, Weiss JH. Zinc: new clues to diverse roles in brain ischemia. Trends in Pharmacological Sciences. 2011; 32(8):480.10.1016/j.tips.2011.04.001 [PubMed: 21621864]
6. Yokoyama M, Koh J, Choi DW. Brief exposure to zinc is toxic to cortical neurons. Neuroscience Letters. 1986; 71:351–355. [PubMed: 3796893]
7. Telford W, Fraker PJ. Preferential induction of apoptosis in mouse CD4+CD8+ alpha betaTCR10CD3e thymocytes by zinc. Journal of Cell Physiology. 1995; 164:259–270.
8. Aizenman E, Stout AK, Hartnett KA, Dinely KE, McLaughlin B, Reynolds IJ. Induction of neuronal apoptosis by thiol oxidation: putative role of intracellular zinc release. Journal of Neurochemistry. 2000; 75(5):1878–1889. [PubMed: 11032877]

$watermark-text
$watermark-text
$watermark-text

9. Bozym RA, Chimienti F, Giblin LJ, Gross GW, Korichneva I, Li Y, et al. Free zinc outside a narrow concentration range is toxic to a variety of cells in vitro. Experimental Biology and Medicine. 2010; 235:741–750.10.1258/ebm.2010.009258 [PubMed: 20511678]
10. Waring P, Egan M, Braithwaite A, Mullbacher N, Siaarda A. Apoptosis induced in macrophages and T-blasts by the mycotoxin sporodesmin and protection by zinc salts. International Journal of Pharmacology. 1990; 12:445–457.
11. Zalewski P, Forbes IJ, Giannakis C. Physiological role for zinc in prevention of apoptosis (gene-directed death). Biochemistry International. 1991; 24:1093–1101. [PubMed: 1781788]
12. Hyun HJ, Sohn JH, Ha DW, Ahn YH, Koh JY, Yoon YH. Depletion of intracellular zinc and copper with TPEN results in apoptosis of cultured human retinal pigment epithelial cells. Invest Ophthalmol Vis Sci. 2001; 42(2):460–465. [PubMed: 11157883]
13. Suh SW, Chen JW, Motamedi M, Bell B, Listiak K, Pons NF, et al. Evidence that synaptically-released zinc contributes to neuronal injury after traumatic brain injury. Brain Research. 2000; 852:268–273. [PubMed: 10678752]
14. Wei G, Hough CJ, Li Y, Sarvey JM. Characterization of extracellular accumulation of Zn2+ during ischemia and reperfusion of hippocampus slices in rat. Neuroscience. 2004; 125:867–877. [PubMed: 15120848]
15. Zeng, H-H.; Bozym, RA.; Rosenthal, RE.; Fiskum, G.; Cotto-Cumba, C.; Westerberg, N., et al. In situ measurement of free zinc in an ischemia model and cell culture using a ratiometric fluorescence-based biosensor. In: Vo-Dinh, T.; Grundfest, WS.; Benaron, DA.; Cohn, GE., editors. SPIE Conference on Advanced Biomedical and CLinical Diagnostic Systems III. Vol. 5692. San Jose, CA: SPIE; 2005. p. 51-59.
16. Frederickson CJ, Giblin LJ, Krezel A, McAdoo DJ, Muelle RN, Zeng Y, et al. Concentrations of extracellular free zinc (pZn)e in the central nervous system during simple anesthetization, ischemia, and reperfusion. Experimental Neurology. 2006; 198:285–293.10.1016/j.expneurol.2005.08.030 [PubMed: 16443223]
17. Stork CJ, Li YV. Intracellular zinc elevation measured with a “calcium-specific” indicator during ischemia and reperfusion in rat hippocampus: A question on calcium overload. Journal of Neuroscience. 2006; 26(41):10430–10437.10.1523/JNEUROSCI.1588-06.2006 [PubMed: 17035527]
18. Tonder N, Johansen FF, Frederickson CJ, Zimmer J, Diemer NH. Possible role of zinc in the selective degeneration of dentate hilar neurons after cerebral ischemia in the adult rat. Neuroscience Letters. 1990; 109:247–252. [PubMed: 2330128]
19. Koh JY, Suh SW, Gwag BJ, He YY, Hsu CY, Choi DW. The role of zinc in selective neuronal death after transient global cerebral ischemia. Science. 1996; 272:1013–1016. [PubMed: 8638123]
20. Yin HZ, Sensi SL, Ogoshi F, Weiss JH. Blockade of Ca2+-permeable AMPA/kainate channels decreases oxygen-glucose deprivation-induced Zn2+ accumulation and neuronal loss in hippocampal pyramidal neurons. Journal of Neuroscience. 2002; 22(4):1273–1279. [PubMed: 11850455]
21. Piantadosi CA, Zhang J. Mitochondrial generation of reactive oxygen species after brain ischemia in the rat. Stroke. 1996; 27:327–332. [PubMed: 8571432]
22. Starkov AA, Fiskum G, Chinopoulos C, Lorenzo BJ, Browne SE, Patel MS, et al. Mitochondrial alpha-Ketoglutarate Dehydrogenase Complex Generates Reactive Oxygen Species. The Journal of Neuroscience. 2004; 24(36):7779–7788.10.1523/jneurosci.1899-04.2004 [PubMed: 15356189]
23. Blomgren H, Hagberg H. Free radicals, mitochondria, and hypoxia-ischemia in the developing brain. Free Radical Biology and Medicine. 2006; 40:388–397. [PubMed: 16443153]
24. Sims NR, Muyderman H. Mitochondria, oxidative metabolism and cell death in stroke. Biochimica et Biophysica Acta. 2010; 1802:80–91. [PubMed: 19751827]
25. Niizuma K, Yoshioka H, Chen H, Kim GS, Jung JE, Katsu M, et al. Mitochondrial and apoptotic neuronal death signaling pathways in cerebral ischemia. Biochimica et Biophysica Acta. 2010; 1802:92–99. [PubMed: 19751828]
26. Bogaert YE, Rosenthal RE, Fiskum G. Postischemic inhibition of cerebral cortex pyruvate dehydrogenase. Free Radical Biology and Medicine. 1994; 16(6):811–820. [PubMed: 8070685]

$watermark-text

$watermark-text

$watermark-text

27. Gazaryan I, Krasnikov BF, Ashby GA, Thorneley RNF, Kristal BS, Brown AM. Zinc is a potent inhibitor of thiol oxidoreductase activity and stimulates reactive oxygen species production by lipoamide dehydrogenase. Journal of Biological Chemistry. 2002; 277(12):10064–10072. [PubMed: 11744691]
28. Gazaryan IG, Krasinskaya IP, Kristal BS, Brown AM. Zinc irreversibly damages major enzymes of energy production and antioxidant defense prior to mitochondrial permeability transition. Journal of Biological Chemistry. 2007; 282:24373–24380.10.107/jbc.M611376200 [PubMed: 17565998]
29. Fierke CA, Thompson RB. Fluorescence-based biosensing of zinc using carbonic anhydrase. Bio Metals. 2001; 14:205–222.
30. Thompson RB, Cramer ML, Bozym R, Fierke CA. Excitation ratiometric fluorescent biosensor for zinc ion at picomolar levels. Journal of Biomedical Optics. 2002; 7(4):555–560. [PubMed: 12421121]
31. Bozym, R.; Hurst, TK.; Westerberg, N.; Stoddard, A.; Fierke, CA.; Frederickson, CJ., et al. Determination of zinc using carbonic anhydrase-based fluorescence biosensors. In: Brand, L.; Johnson, M., editors. Fluorescence Spectroscopy. Vol. 450. San Diego: Academic Press; 2008. p. 287-309.Methods in Enzymology
32. Hurst TK, Wang D, Thompson RB, Fierke CA. Carbonic anhydrase II-based metal ion sensing: Advances and new perspectives. Biochimica et Biophysica Acta (BBA) - Proteins & Proteomics. 2010; 1804(2):393–403.
33. Wang D, Hurst TK, Thompson RB, Fierke CA. Genetically encoded ratiometric biosensors to measure extracellular exchangeable zinc in Escherichia coli. Journal of Biomedical Optics. 2011; 16(8) 087011-087011–087011-087011. 10.1117/1.3613926
34. Huang, C-c; Lesburg, CA.; Kiefer, LL.; Fierke, CA.; Christianson, DW. Reversal of the hydrogen bond to zinc ligand histidine-119 dramatically diminishes catalysis and enhances metal equilibration kinetics in carbonic anhydrase II. Biochemistry. 1996; 35(11):3439–3446. [PubMed: 8639494]
35. Hunt JA, Ahmed M, Fierke CA. Metal binding specificity in carbonic anhydrase is influenced by conserved hydrophobic amino acids. Biochemistry. 1999; 38:9054–9060. [PubMed: 10413479]
36. McCall KA, Fierke CA. Probing determinants of the metal ion selectivity in carbonic anhydrase using mutagenesis. Biochemistry. 2004; 43:3979–3986. [PubMed: 15049705]
37. Bozym RA, Thompson RB, Stoddard AK, Fierke CA. Measuring picomolar intracellular exchangeable zinc in PC-12 cells using a ratiometric fluorescence biosensor. ACS Chemical Biology. 2006; 1(2):103–111. [PubMed: 17163650]
38. Stumm, W.; Morgan, JJ. Aquatic Chemistry: Chemical Equilibria and Rates in Natural Waters. 3. New York: Wiley-Interscience; 1996.
39. Prasad AS, Oberleas D. Zinc in human serum: evidence for an amino acid-bound fraction. Journal of Laboratory and CLinical Medicine. 1968:1006.
40. Peck EJ, Ray WJ. Metal complexes of phosphoglucomutase in vivo: alterations induced by insulin. Journal of Biological Chemistry. 1971; 246(4):1160–1167. [PubMed: 5543683]
41. Krezel A, Maret W. Zinc-buffering capacity of a eukaryotic cell at physiological pZn. Journal of Biological Inorganic Chemistry. 2006; 11:1049–1062. [PubMed: 16924557]
42. Sensi SL, Ton-That D, Weiss JH, Rothe A, Gee KR. A new mitochondrial fluorescent zinc sensor. Cell Calcium. 2003; 34(3):281–284. [PubMed: 12887975]
43. Masanta G, Lim CS, Kim HJ, Han JH, Kim HM, Cho BR. A Mitochondrial-Targeted Two-Photon Probe for Zinc Ion. Journal of the American Chemical Society. 2011; 133(15):5698. [PubMed: 21449534]
44. Dittmer PJ, Miranda JG, Gorski JA, Palmer AE. Genetically encoded sensors to elucidate spatial distribution of cellular zinc. Journal of Biological Chemistry. 2009; 284:16289–16297.10.1074/jbc.M900501200 [PubMed: 19363034]
45. Caporale T, Ciavardelli D, Di Ilio C, Lanuti P, Drago D, Sensi SL. Ratiometric-pericam-mt, a novel tool to evaluate intramitochondrial zinc. Experimental Neurology. 2009; 218(2):228. [PubMed: 19374897]

$watermark-text

$watermark-text

$watermark-text

46. Danilov C, Fiskum G. Hyperoxia promotes astrocyte cell death after oxygen and glucose deprivation. Glia. 2008 in the press.
47. Lindskog, S.; Henderson, LE.; Kannan, KK.; Liljas, A.; Nyman, PO.; Strandberg, B. Carbonic anhydrase. In: Boyer, PD., editor. The Enzymes. Vol. 5. New York: Academic Press; 1971. p. 587-665.The Enzymes
48. Jiang Z-G, Lu XCM, Nelson V, Yang X, Pan W, Chen R-w, et al. A multifunctional cytoprotective agent that reduces neurodegeneration after ischemia. Proceedings of the National Academy of Sciences of the United States of America. 2006; 103(5):1581–1586.10.1073/pnas.0510573103 [PubMed: 16423893]
49. Thompson RB Jr, WOW, Maliwal BP, Fierke CA, Frederickson CJ. Fluorescence microscopy of stimulated Zn(II) release from organotypic cultures of mammalian hippocampus using a carbonic anhydrase-based biosensor system. Journal of Neuroscience Methods. 2000; 96(1):35–45. [PubMed: 10704669]
50. Haase H, Hebel S, Engelhardt G, Rink L. Flow cytometric measurement of labile zinc in peripheral blood mononuclear cells. Analytical Biochemistry. 2006; 352(2):222. [PubMed: 16545333]
51. Haase H, Ober-BlÃ¶baum JL, Engelhardt G, Hebel S, Heit A, Heine H, et al. Zinc Signals Are Essential for Lipopolysaccharide-Induced Signal Transduction in Monocytes. The Journal of Immunology. 2008; 181(9):6491–6502. [PubMed: 18941240]
52. Rudolf E, Červinka M. Zinc pyrithione induces cellular stress signaling and apoptosis in Hep-2 cervical tumor cells: the role of mitochondria and lysosomes. Bio Metals. 2010; 23(2):339–354.
53. Haase, H.; Rink, L. Zinc signaling. In: Rink, L., editor. Zinc in Human Health. Amsterdam: IOS press; 2011.
54. Atar D, Backx PH, Appel MM, Gao WD, Marban E. Excitation-Transcription Coupling Mediated by Zinc Influx through Voltage-dependent Calcium Channels. Journal of Biological Chemistry. 1995; 270(6):2473–2477.10.1074/jbc.270.6.2473 [PubMed: 7852308]
55. Ayaz M, Turan B. Selenium prevents diabetes-induced alterations in [Zn2+]i and metallothionein level of rat heart via restoration of cell redox cycle. American Journal of Physiology - Heart and Circulatory Physiology. 2006; 290(3):H1071–H1080.10.1152/ajpheart.00754.2005 [PubMed: 16214842]
56. Sensi SL, Canoniero LMT, Yu SP, Ying HS, Koh JY, Kerchner GA, et al. Measurement of intracellular free zinc in living cortical neurons: routes of entry. Journal of Neuroscience. 1997; 17(24):9554–9564. [PubMed: 9391010]
57. Thompson RB, Peterson D, Mahoney W, Cramer M, Maliwal BP, Suh SW, et al. Fluorescent zinc indicators for neurobiology. Journal of Neuroscience Methods. 2002; 118:63–75. [PubMed: 12191759]
58. Dongen, EMWMv; Evers, TH.; Dekkers, LM.; Meijer, EW.; Klomp, LWJ.; Merkx, M. Variation of linker length in ratiometric fluorescent sensor proteins allows rational tuning of Zn(II) affinity in the picomolar to femtomolar range. Journal of the American Chemical Society. 2007; 129:3494–3495.10.1021/ja069105 [PubMed: 17335212]
59. Qin Y, Dittmer PJ, Park JG, Jansen KB, Palmer AE. Measuring steady-state and dynamic endoplasmic reticulum and Golgi Zn2+ with genetically encoded sensors. Proceedings of the National Academy of Sciences. 201110.1037/pnas.1015686108
60. Sensi SL, Yin HZ, Carriedo SG, Rao SS, Weiss JH. Preferential Zn2+ influx through Ca2+-permeable AMPA/kainate channels triggers prolonged mitochondrial superoxide production. Proceedings of the National Academy of Sciences. 1999; 96:2414–2419.
61. Weiss JH, Sensi S. Ca2+ - Zn2+ permeable AMPA or kainate receptors: possible key factors in selective neurodegeneration. Trends in Neuroscience. 2000; 23(8):365–371.
62. Soane, L.; Polster, BM.; Fiskum, G. Mitochondrial mechanisms of neural cell death in cerebral ischemia. In: Reed, JC.; Green, D., editors. Apoptosis: Physiology and Pathology of Cell Death. Cambridge: Cambridge University Press; 2010.
63. Fiskum G, Murphy AN, Beal MF. Mitochondria in neurodegeneration: Acute ischemia and chronic neurodegenerative diseases. Journal of Cerebral Blood Flow and Metabolism. 1999; 19:351–369. [PubMed: 10197505]

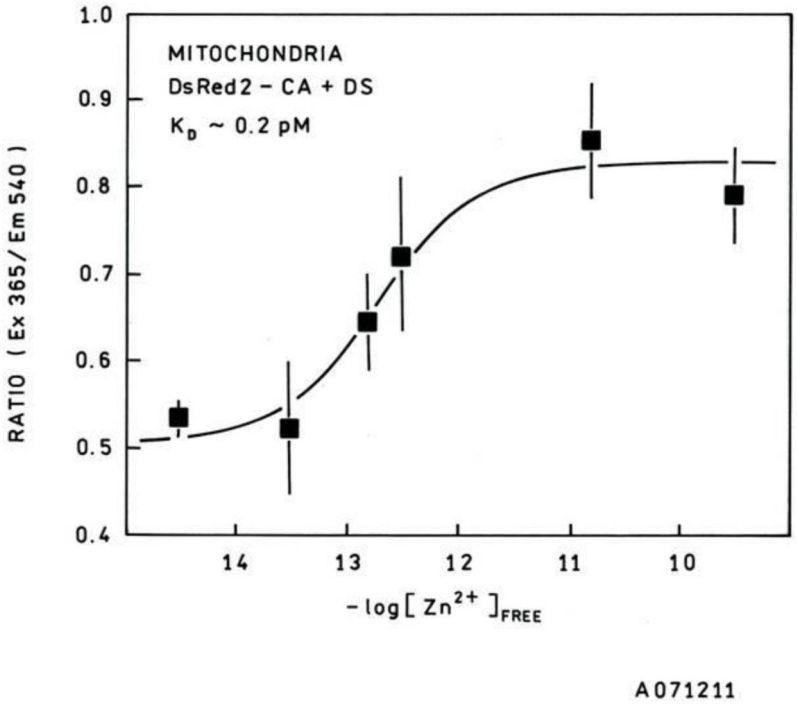

Figure 1.

Calibration curve for apoCA-DsRed2 expressed in isolated transfected mitochondria (closed squares). The best fit curve shows tighter binding for zinc in isolated mitochondria (K_d = 0.2 *pM*) compared with ordinary buffers at physiological pH and ionic strength (K_d = 17 *pM*). The dynamic range for the mitochondrial targeted probe is roughly from 0.02 *pM* to 2 *pM*.

$watermark-text
$watermark-text
$watermark-text

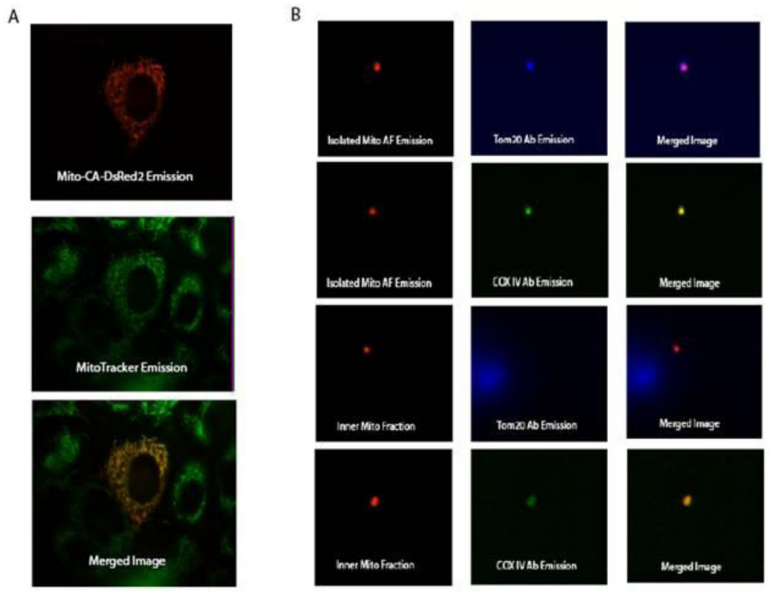

Figure 2.

Co-localization of Mito-CA-DsRed2. A.) Co-localization of the mitochondrial targeted probe (pseudocolored red) and the MitoTracker probe (pseudocolored green). The yellow color in the merged image indicates that probe successfully targets the mitochondria of transfected cells. B.) Co-localization of the mitochondrial target probe and antibodies specific for the outer mitochondrial membrane (TOM20) and inner mitochondrial membrane (COX IV). Co-localization experiments were performed on both whole isolated mitochondria and inner mitochondrial membrane/matrix fractions. Incubation with the antibodies suggests that the Mito-CA-DsRed2 sensor is expressed in the inner mitochondrial membrane/matrix of transfected cells.

$watermark-text
$watermark-text
$watermark-text

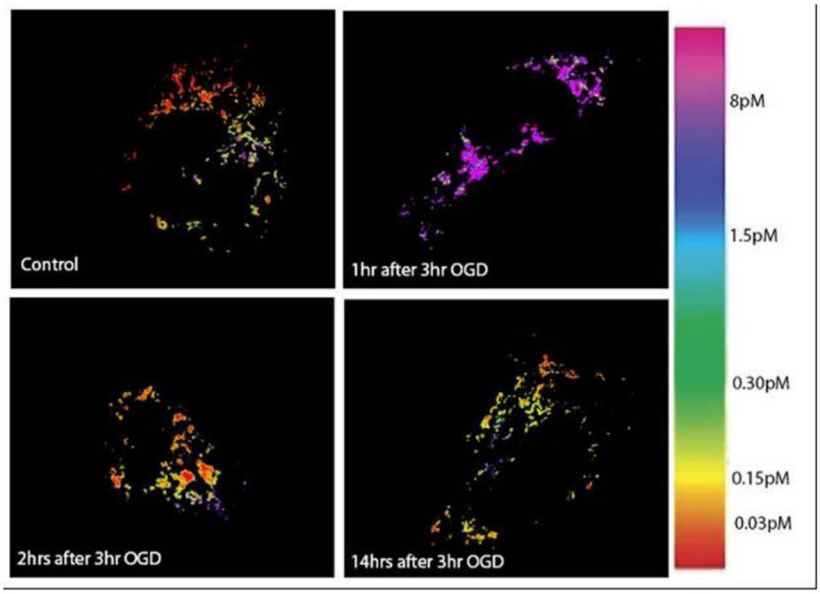

Figure 3.

Pseudocolored Ratio Images of Mitochondrial Free [Zn] Following OGD. Physiological conditions (top left), 1 hr after OGD (top right), 2 hrs after OGD (bottom left), 14 hrs after OGD (bottom right). The images clearly show an increase in free zinc in the mitochondria at 1 hr after OGD, and a return to physiological levels shortly thereafter.

$watermark-text
$watermark-text
$watermark-text

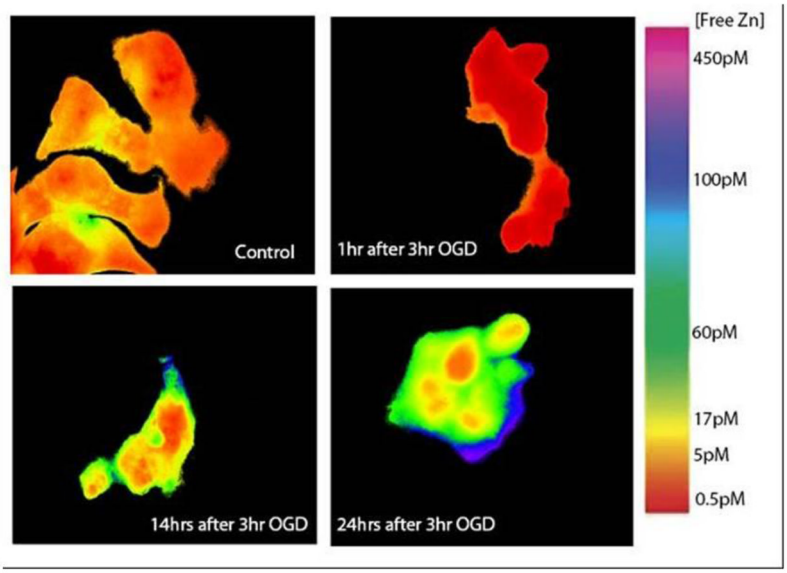

Figure 4.
Changes in cytoplasmic free zinc following OGD. Pseudocolored ratio images following 3 hr OGD insult in PC12 cells. Physiological Conditions (top left), 1 hr after OGD (top right), 14 hrs after OGD (bottom left), 24 hrs after OGD (bottom right). Images indicate that intracellular zinc decreases after OGD before increasing gradually over a 24 hour time period.

$watermark-text
$watermark-text
$watermark-text

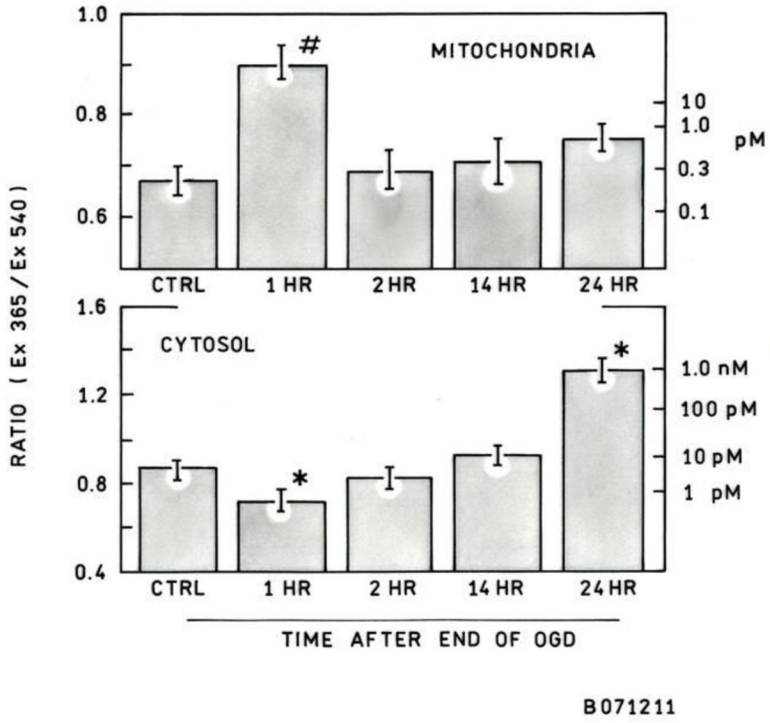

Figure 5.

Cytosolic and mitochondrial matrix free zinc concentrations following OGD. The average ratio of Ex365*nm*/Ex540*nm* was calculated for each cell (left scale), and from this ratio the zinc concentration could be determined using the calibration curve (right scale). After OGD there is a decrease in cytosolic zinc followed by a gradual increase. Mitochondrial matrix zinc increases significantly 1 hr after OGD and then returns to near physiological levels. The increase in matrix zinc occurs at the same time as the decrease in cytosolic zinc is observed. Error bars represent the standard error of the mean. $n_{cytosol}$ = 70–90 cells, n_{mito} = 35–45 cells, * $p < 0.05$, # $p < 0.01$.

$watermark-text
$watermark-text
$watermark-text